Supporting Information for

Electronically Modulated Cobalt-Nitrogen/Carbon Catalyst via Ligand Displacement of Metal-Organic Frameworks toward Efficient Oxygen Reduction

Pengcheng Wan,[a] Bin Li,[b] Yihang Tang,[c] Xu Zeng,[a] Yulong Wu,[a] Junlong Yao,[a] Junwu Xiao,*[b] Bao Yu Xia,*[b] Yimin Sun*[a]

[a]*Hubei Key Laboratory of Plasma Chemistry and Advanced Materials, School of Materials Science and Engineering, Wuhan Institute of Technology, Wuhan 430205, China*

[b]*Key Laboratory of Material Chemistry for Energy Conversion and Storage, Ministry of Education, School of Chemistry and Chemical Engineering, Huazhong University of Science & Technology, Wuhan 430074, China*

[c]*College of Food Science and Technology, Huazhong Agricultural University, Wuhan, Hubei, 430070, China*

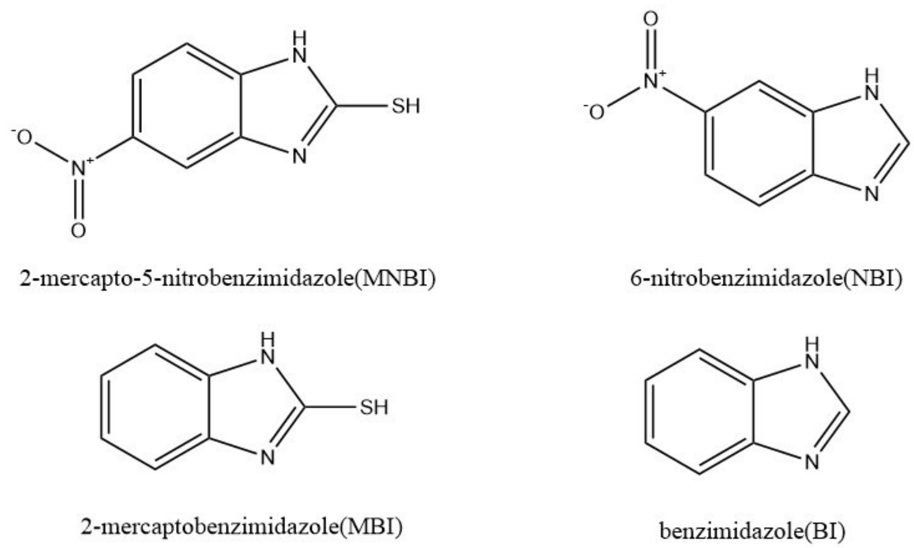

Fig. S1 Chemical structures of ligands.

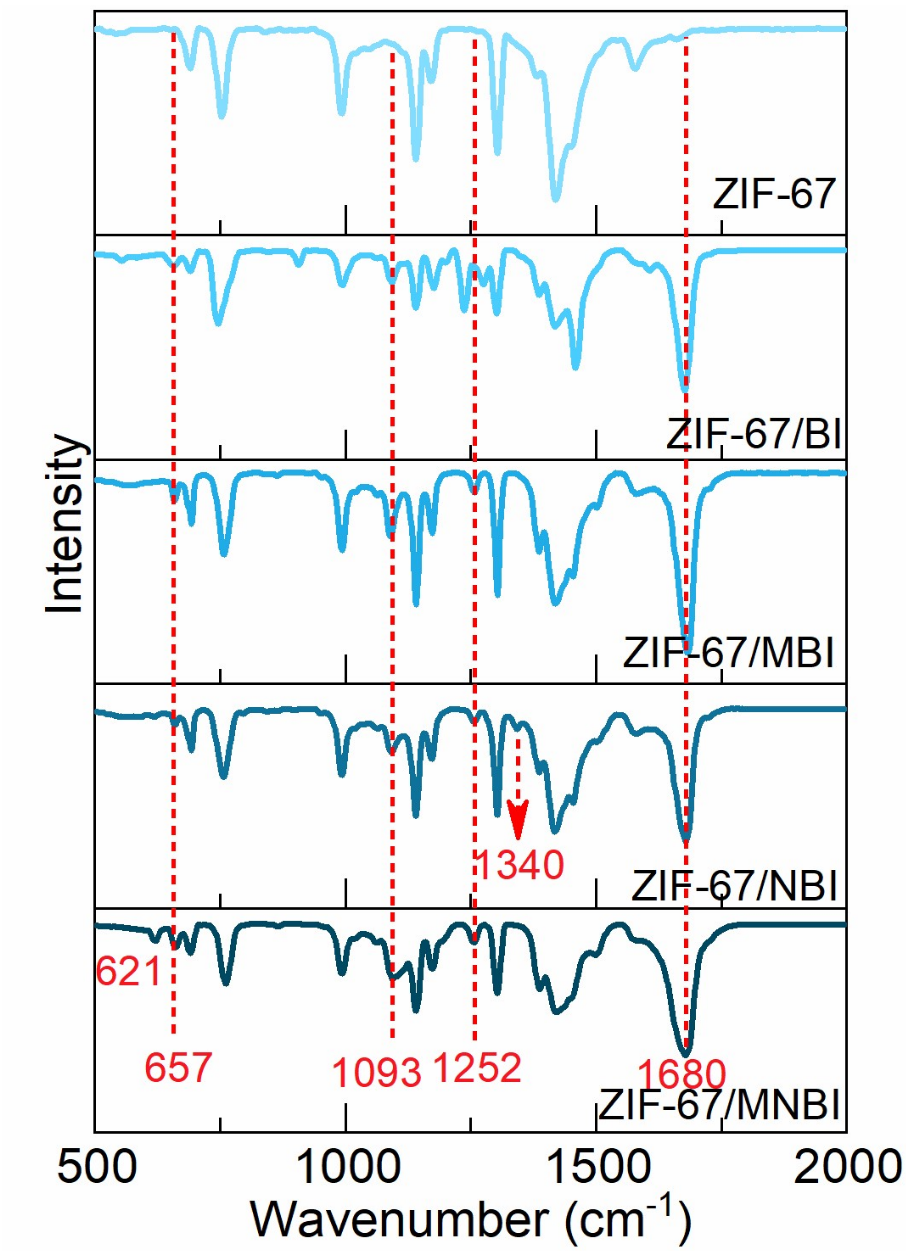

Fig. S2 FT-IR spectra of ZIF-67 and ZIF-67/X.

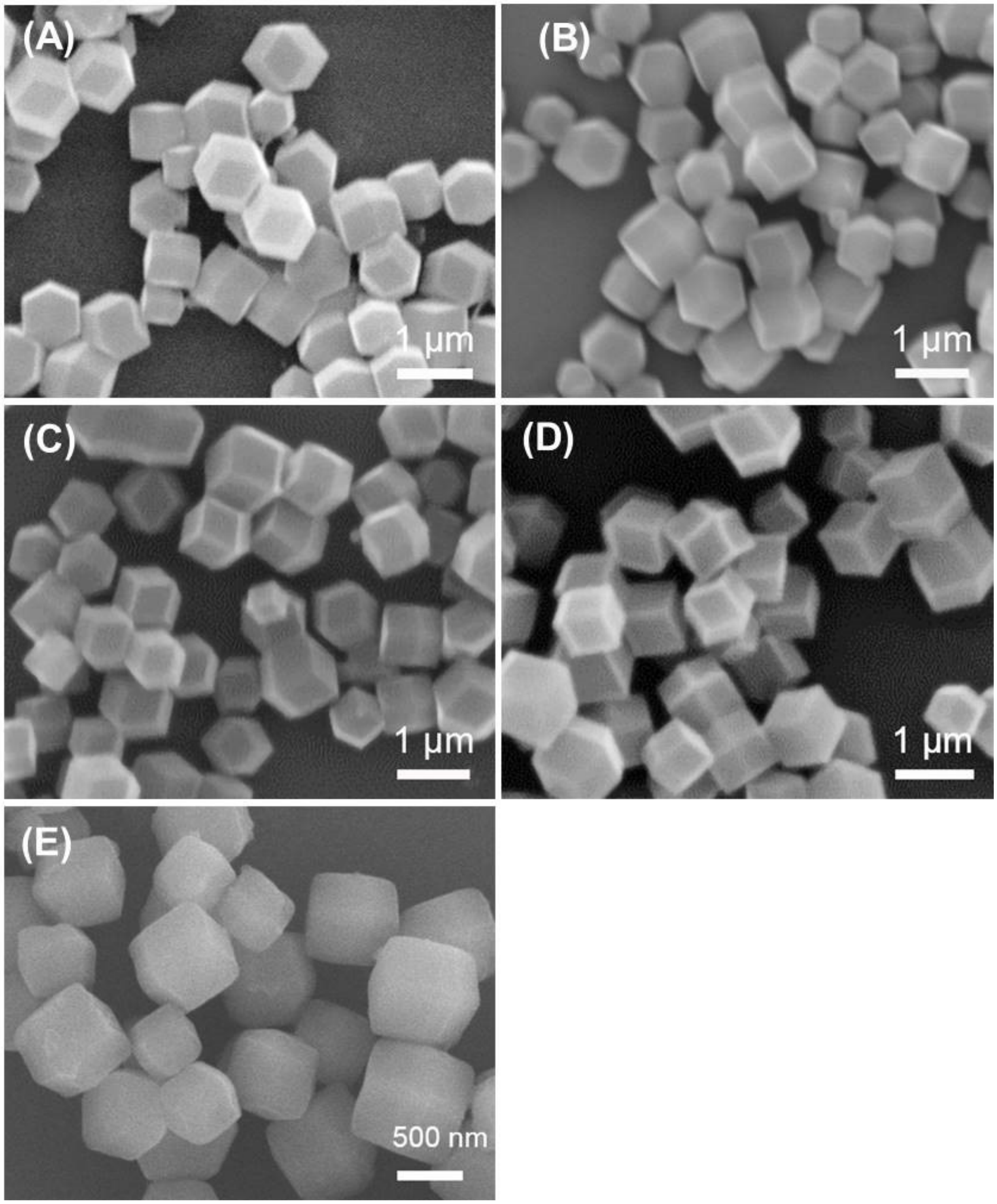

Fig. S3 SEM images of (A) ZIF-67, (B) ZIF-67/BI, (C) ZIF-67/MBI, (D) ZIF-67/NBI and (E) ZIF-67/MNBI.

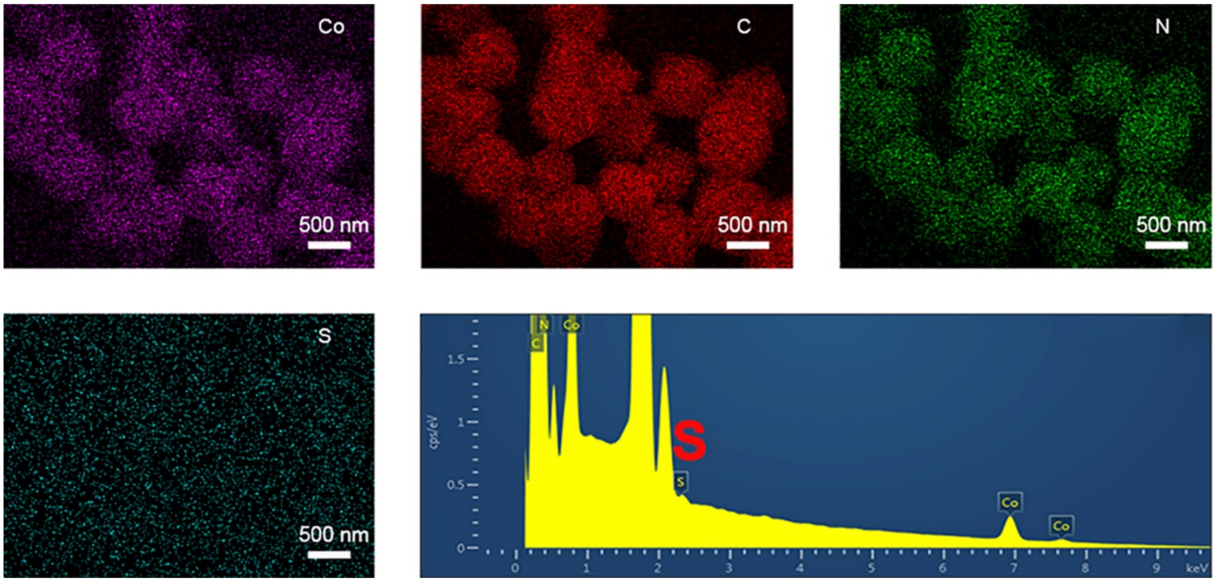

Fig. S4 EDS mapping analysis of ZIF-67/MNBI.

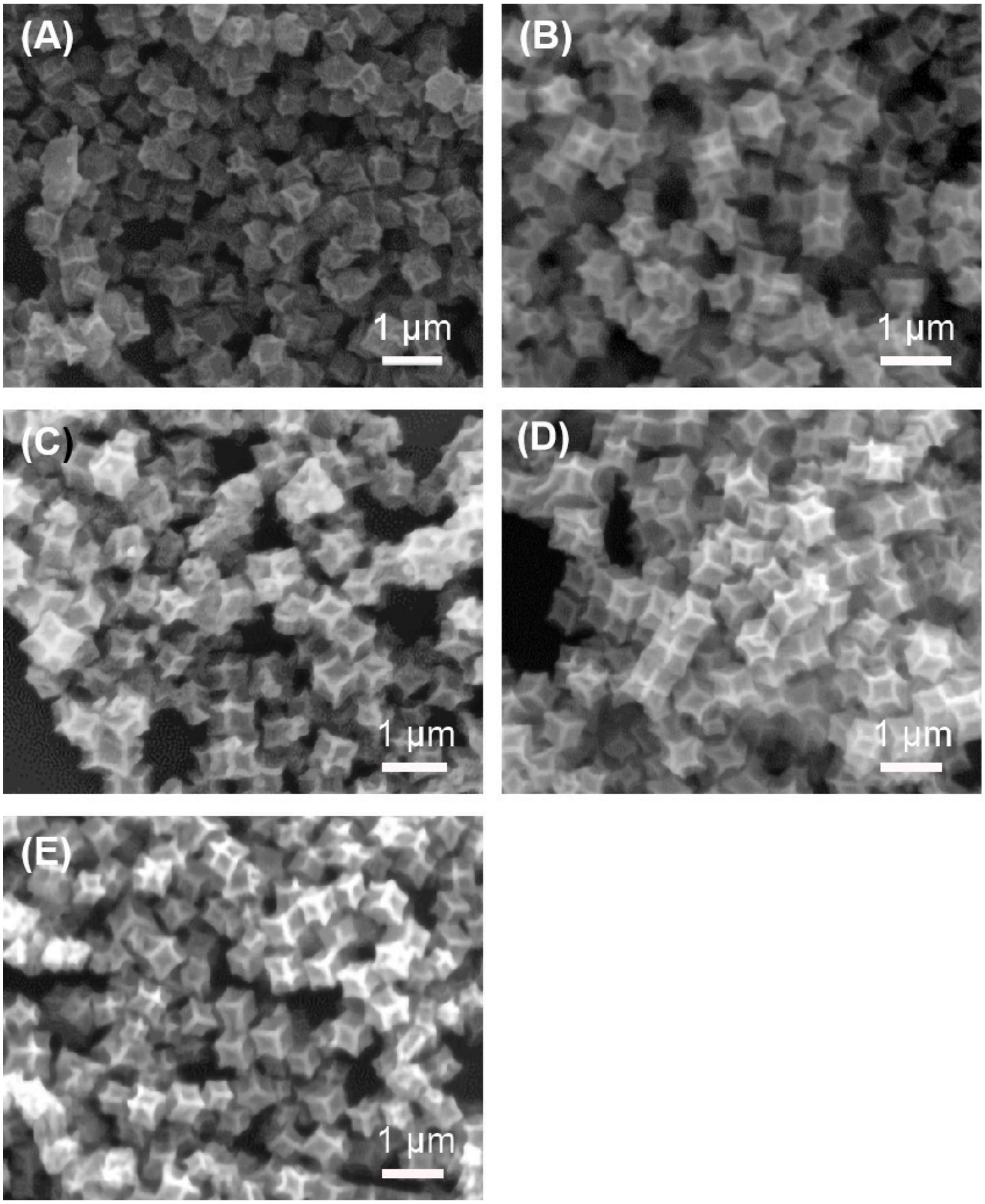

Fig. S5 SEM images of (A) ZIF-67-800, (B) ZIF-67/BI-800, (C) ZIF-67/NBI-800, (D) ZIF-67/MNI-800, (E) ZIF-67/MNBI-800.

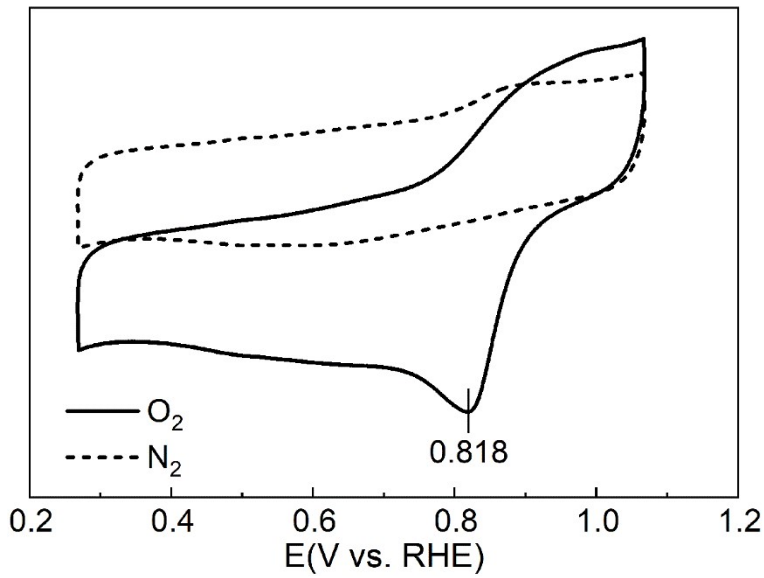

Fig. S6 CV curves of Pt/C catalyst with a loading of 20 μg_{Pt} cm^{-2} in N_2 (dash line) or O_2 (solid line)-saturated 0.1 M KOH solution.

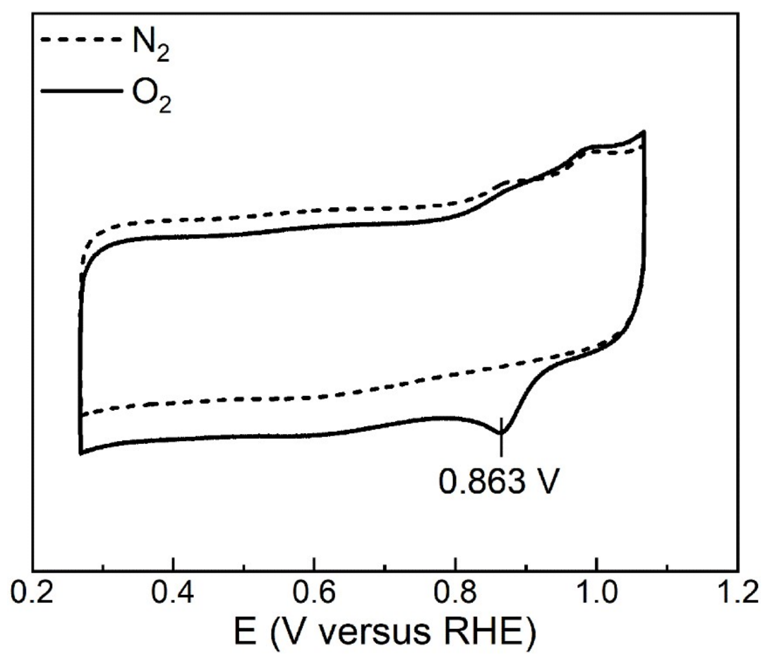

Fig. S7 CV curves of A-ZIF-67/MNBI-800 catalyst in N_2 or O_2-saturated 0.1 M KOH solution (Solid line: O_2; Dash line: N_2).

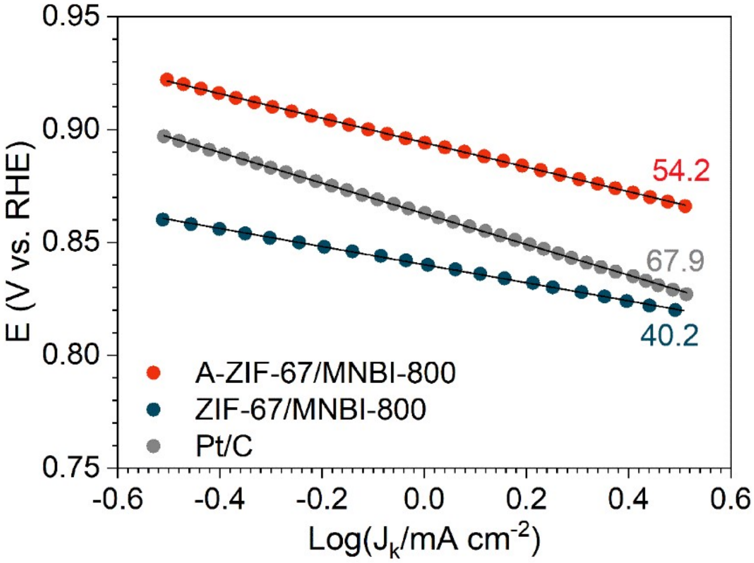

Fig. S8 Tafel curves of ZIF-67/MNBI-800, A-ZIF-67/MNBI-800, and Pt/C catalysts.

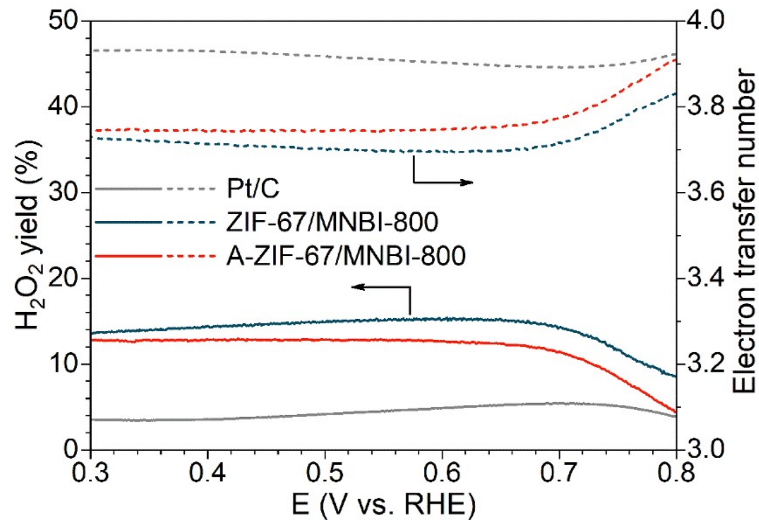

Fig. S9 H_2O_2 yield (HO_2^-%) and electron transfer number (*n*) under the catalysis of ZIF-67/MNBI-800, A-ZIF-67/MNBI-800 and Pt/C catalysts (Solid lines: H_2O_2 yield; Dash lines: electron transfer number), which are acquired from the rotating ring-disk electrode (RRDE) according to the following equations:

$$HO_2^-\% = \frac{(200 \times I_r)}{(I_d \times N + I_r)} \quad (1)$$

$$n = \frac{(4 \times I_d)}{(I_d + {}^{I_r}/_{N})} \quad (2)$$

where I_r and I_d respresent the ring and disk current, respectively, and N is ring collection efficiency ($N = 0.42$).

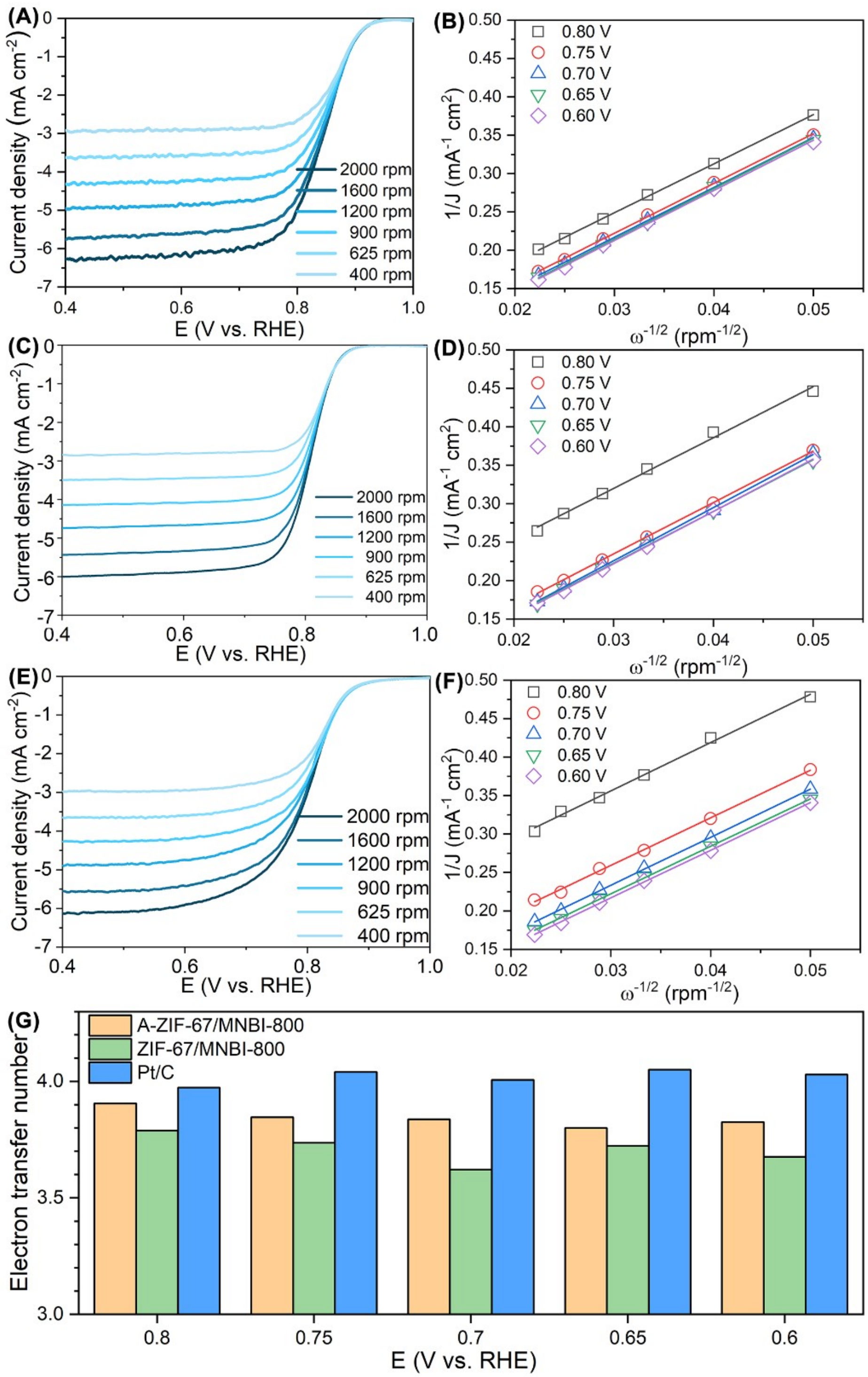

Fig. S10 LSV curves and K-L plots of (A, B) A-ZIF-67/MNBI-800, (C, D) ZIF-67/MNBI-800, and (E, F) Pt/C catalysts, and (G) corresponding electron transfer number at a potential of 0.80–0.60 V versus RHE that were determined from the Koutecky-Levich (K-L) plots on the basis of eqs (3)–(5):

$$\frac{1}{J} = \frac{1}{J_L} + \frac{1}{J_k} \tag{3}$$

$$J_L = 0.20nFC_0(D_0)^{3/2}v^{-1/6}\omega^{1/2} \tag{4}$$

$$J_k = nFKC_0 \tag{5}$$

where J, J_L and J_k are the measured, diffusion-limited and kinetic current densities, respectively, ω is the electrode rotation rate (rpm), F is the Faraday constant (F = 96,485 C mol^{-1}), n is the electron transferred number for oxygen reduction, C_0 is the oxygen-saturated concentration (1.26 × 10^{-6} mol cm^{-3}), D_0 is the oxygen diffusion coefficient in 0.1 M KOH (1.73 × $10^{-5}$$cm^2$ s^{-1}), v is the kinetic viscosity of the solution (1.09 × 10^{-2} cm^2 s^{-1}) and K is the rate constant of the reaction.

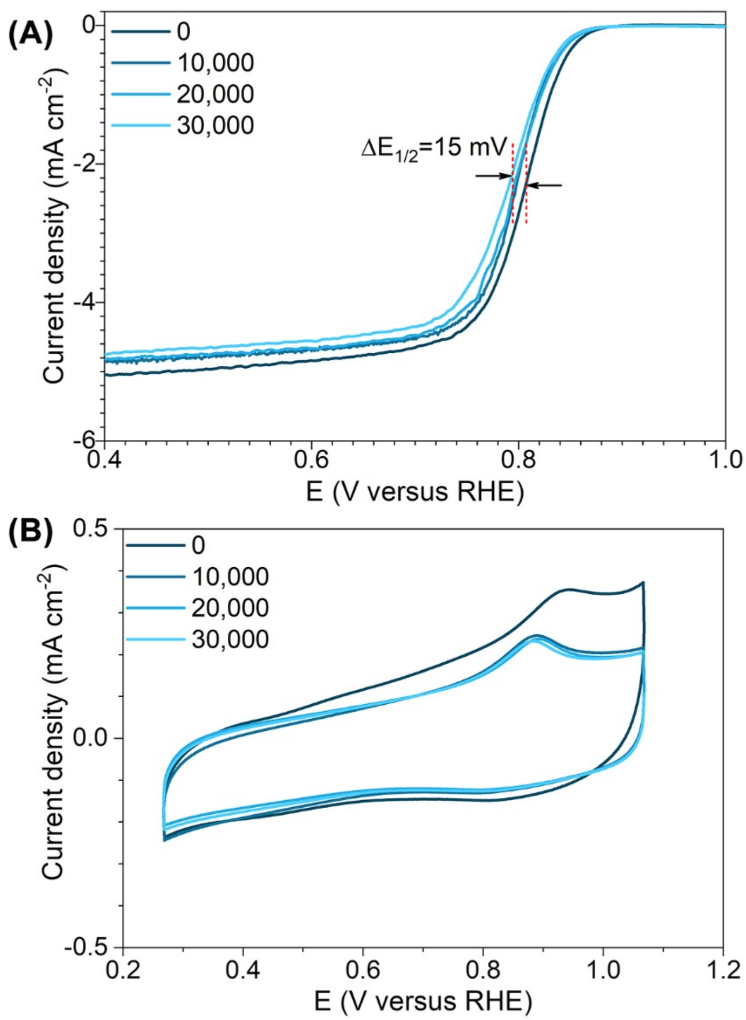

Fig. S11 RDE stability test of ZIF-67/MNBI-800 catalyst in O_2-saturated 0.1 M KOH using the ADT protocol and corresponding CV curves in N_2-saturated 0.1 M KOH solution.

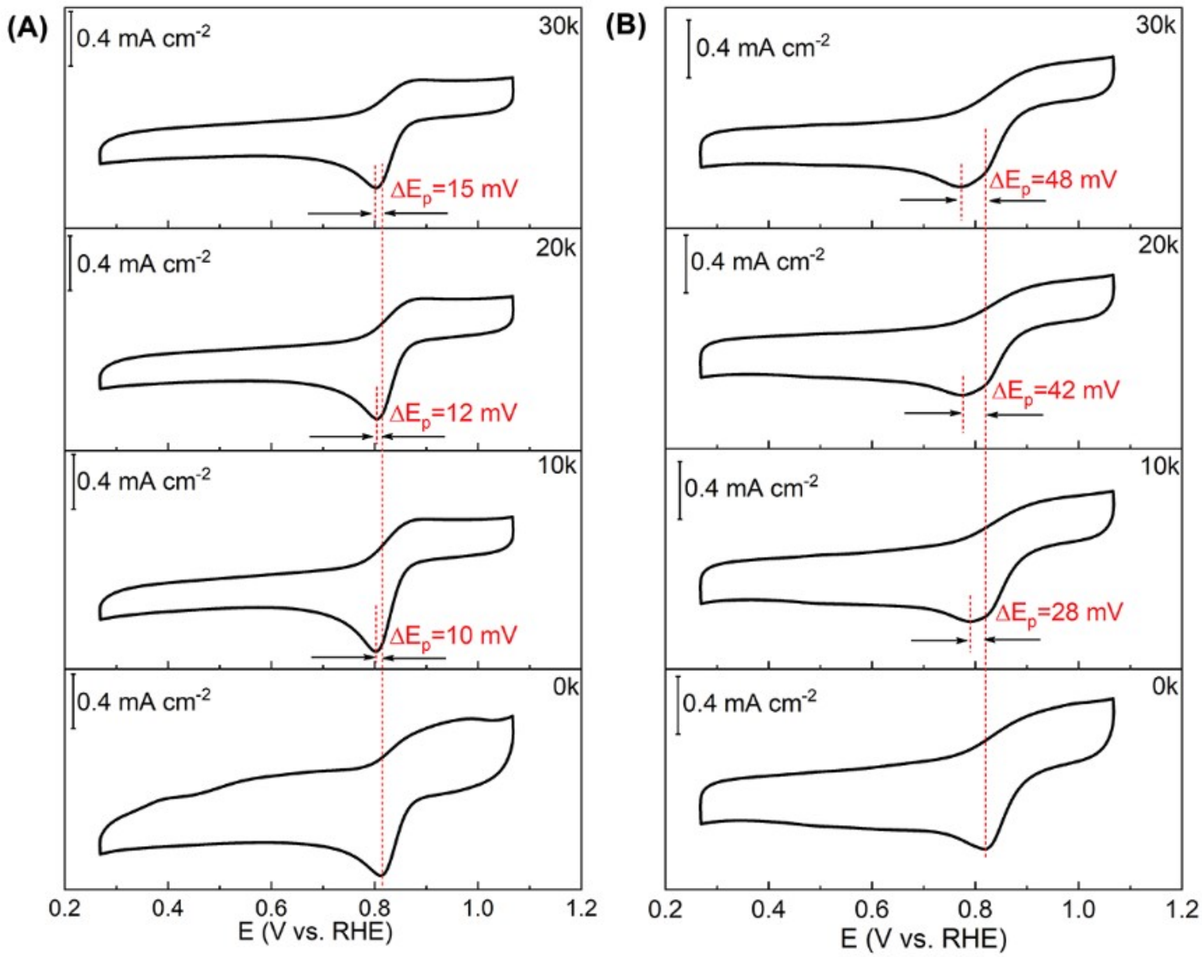

Fig. S12 CV curves of (A) ZIF-67/MNBI-800 and (B) Pt/C catalysts in O_2-saturated 0.1 M KOH solution during the ADT.

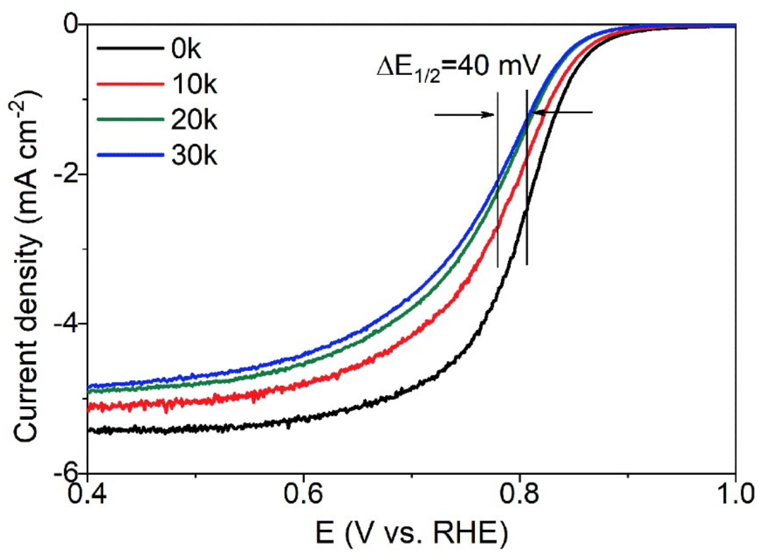

Fig. S13 RDE stability test of Pt/C catalyst in O_2-saturated 0.1 M KOH using the ADT protocol.

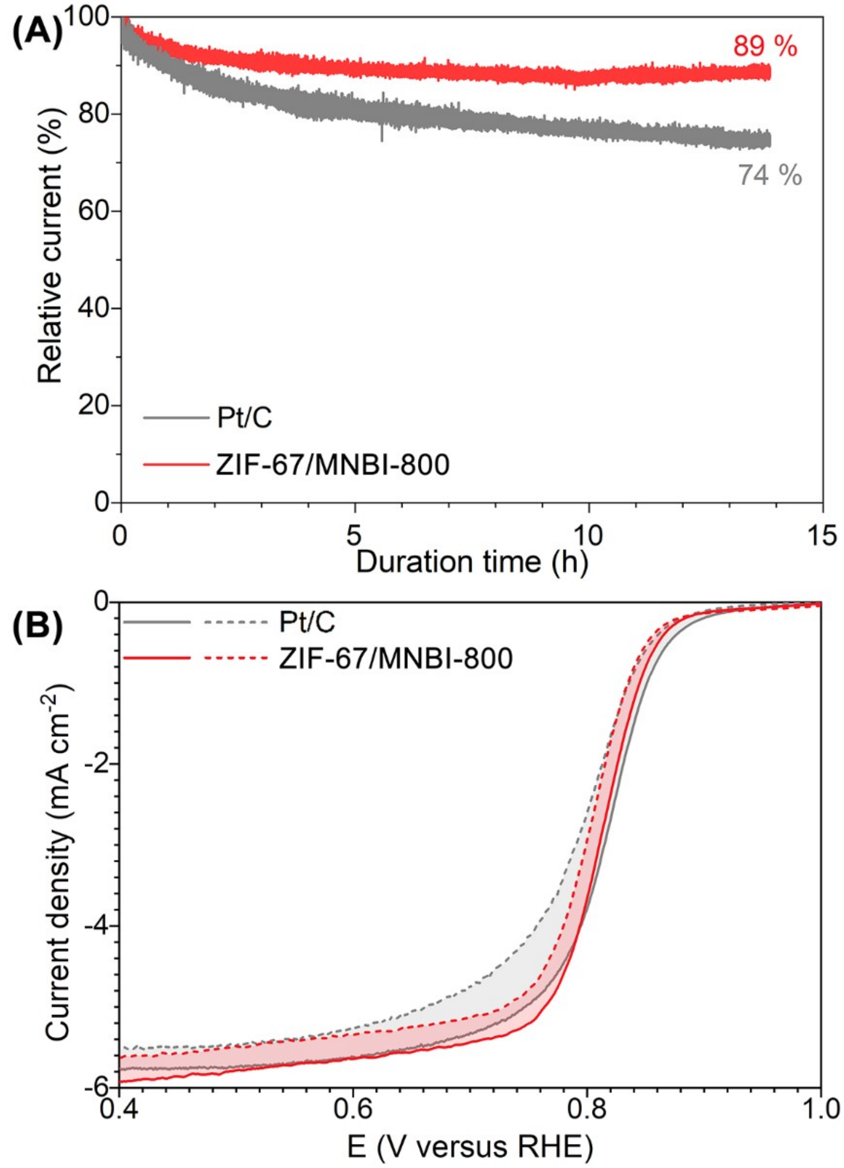

Fig. S14 Chronoamperometric response of Pt/C and ZIF-67/MNBI-800 catalysts, which are measured in O_2-saturated 0.1 M KOH solution and at 0.5 V versus RHE, and corresponding LSV curves (Solid lines: 0 h; Dash lines: 14 h).

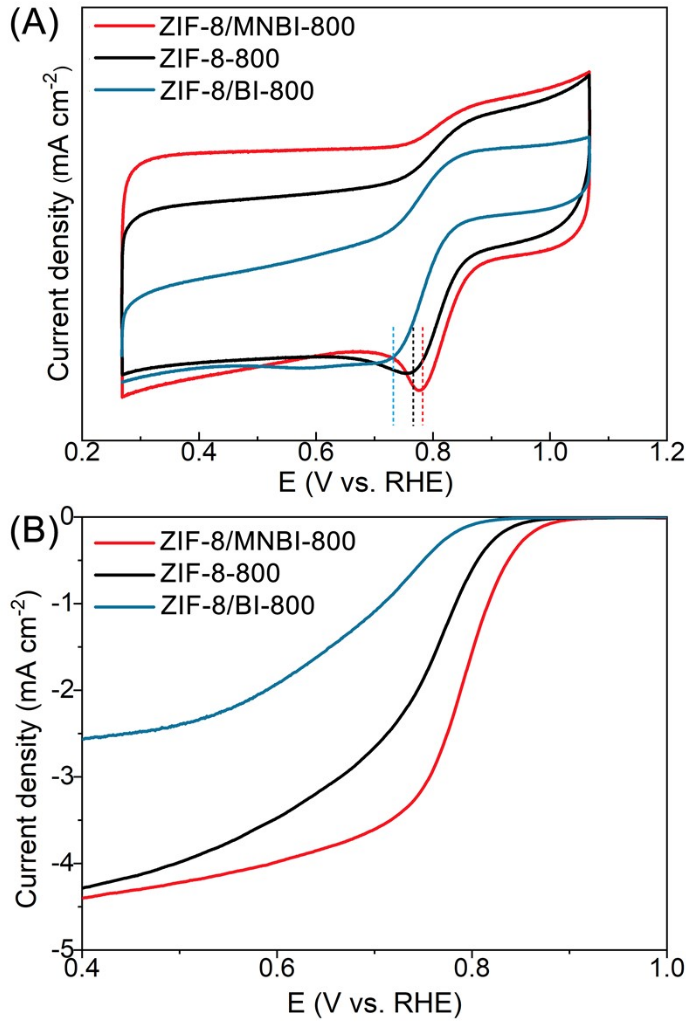

Fig. S15 (A) CV and (B) LSV curves of ZIF-8/BI-800, ZIF-8-800, and ZIF-8/MNBI-800 catalysts in O_2-saturated 0.1 M KOH solution.

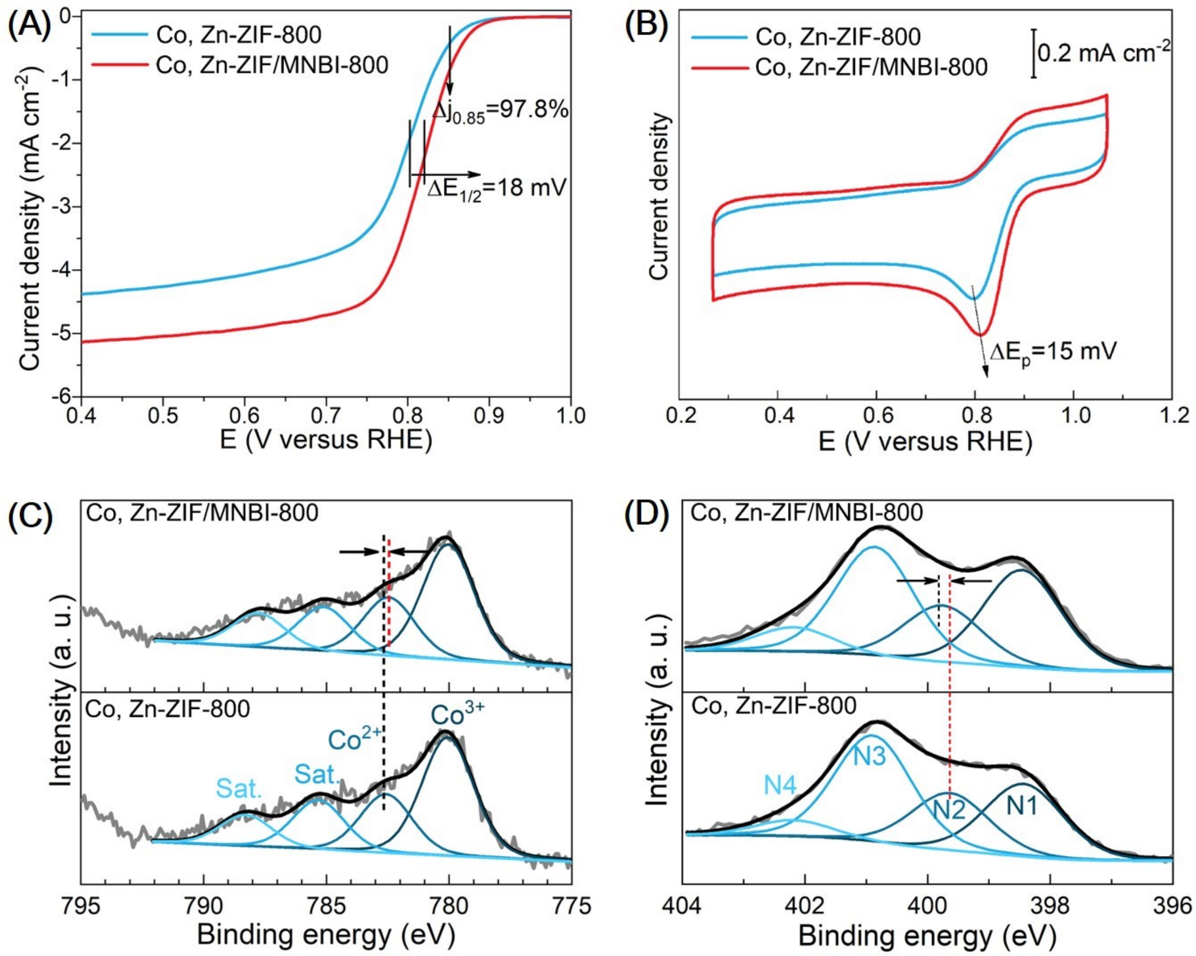

Fig. S16 (A) LSV and (B) CV curves of Co, Zn-ZIF-800 and Co, Zn-ZIF/MNBI-800 catalysts carried out in O_2–saturated 0.1 M KOH solution; High-resolution XPS spectra of Co, Zn-ZIF/MNBI-800 and Co, Zn-ZIF-800 and in (C) Co 2p and (D) N 1s regions.

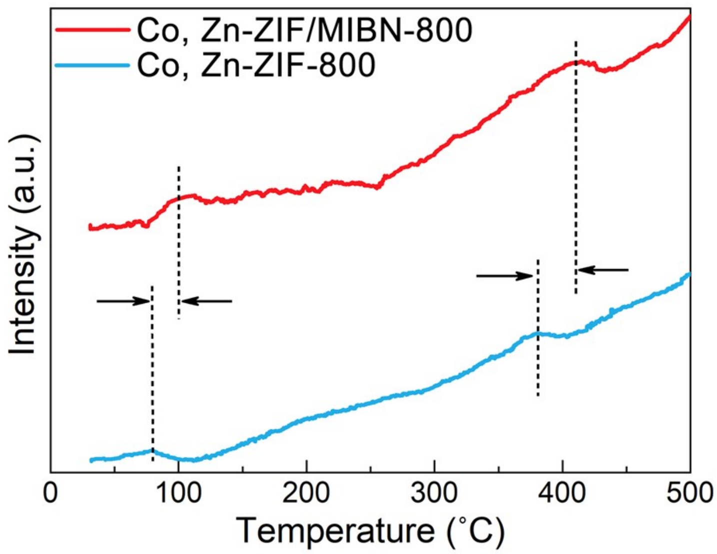

Fig. S17 O_2-TPD profiles of Co, Zn-ZIF-800 and Co, Zn-ZIF/MNBI-800 catalysts.

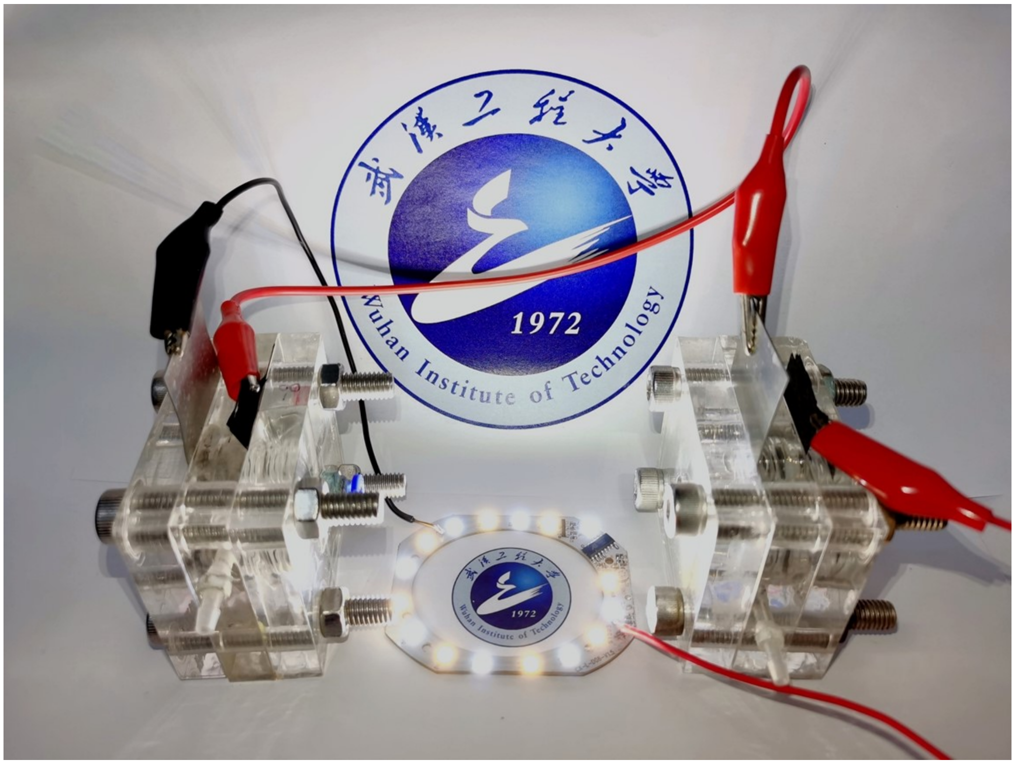

Fig. S18 Digital image of 52 blue light-emitting diodes powered by two series-connected zinc-air batteries driven by A-ZIF-67/MNBI-800 air cathode.

Table S1. The Co Contents (wt%) in ZIF-67/X-800 and A-ZIF-67/MNBI-800 determined by Microwave Plasma-atom Emission Spectrometer (MP-AES).

Samples	Co(%)
ZIF-67/MNBI-800	20.3
ZIF-MBI-800	22.1
ZIF-NBI-800	26.5
ZIF-BI-800	25.2
ZIF-67-800	22.5
A-ZIF-67/MNBI-800	12.4

Table S2. Comparison of ORR Activities Including Catalyst Loading (m, mg cm^{-2}), Onset Potential (E_{onset} Versus RHE), Half-wave Potential ($E_{1/2}$ Versus RHE), as well as Tafel Slope (*b*, mV dec^{-1}) of ZIF-67/MNBI-800, A-ZIF/MNBI-800 and Zinc-air Battery Performance Including Peak Power Density (PPD, mW cm^{-2}) and Long-term Durability at 5 mA cm^{-2} with MOF-derived Catalysts Reported in Recent Years.

Catalysts	ORR activity				Zinc-air battery		References
	Loading	E_{onset}	$E_{1/2}$	*b*	PPD	Durability	
ZIF-67/MNBI-800	0.1	0.88	0.810	40.1	249.7	740 h	This work
A-ZIF-67/MNBI-800	0.1	0.94	0.849	54.2	302.0	750 h	This work
P-Fe-N-CNTs	1	1.04	0.8843	69	145.0	140 h(10 mA cm^{-2})	1
$CoFe_2O_4$/NPC	1	1.08	0.898	65	269.0	700 h (10 mA cm^{-2})	2
Co_2P/doped-CNTs	4	1.603	0.843	55	193.0	50 h (10 mA cm^{-2})	3
CoFe@NOC	1	0.955	0.853	76.9	205.7	100 h	4
Co_2P@NPC	1	1.225	0.852	48.8	198.1	130 h (10 mA cm^{-2})	5
Fe,$CoZn_{9+9}$-NO/WC	2	1.041	0.889	84.2	190.0	290 h (10 mA cm^{-2})	6
FeM/G/H	1	N/A	0.8	90.2	170.1	72 h (10 mA cm^{-2})	7
FeP-NWCC	N/A	1.54	0.86	74	144.0	450 h (10 mA cm^{-2})	8
mFeNC-CNT	1	1.029	0908	56.1	108.0	797 h (10 mA cm^{-2})	9
FePc@NC-1000	1	0.99	0.86	44.41	120.4	N/A	10
Cu/Fe/N-CNS	1	N/A	0.91	66	76.4	150 h (15 mA cm^{-2})	11
Co_9S_8/Co–Nx/CoNi/Ni_3S_2@ CNS-4	1	N/A	**0.**86	79	206.9	400 h (10 mA cm^{-2})	12
Fe-N-C/rGO	0.58	0.99	0.90	61	107.1	400 h	13
ZnCo-NC-II	1	0.97	0.86	67.35	161.8	802 h	14
CoSAs-NGST	N/A	0.99	0.89	65	148	133 h	15

References

1. H. Chang, Y. F. Guo, X. Liu, P. F. Wang, Y. Xie, T. F. Yi, Applied Catalysis B: Environmental., 2023, 327,122469.
2. X. Dong, P. Sun, J. Wu, et al. Adv Compos Hybrid Mater., 2023, 6, 72.
3. L. Song, H. Fan, X. Fan, H. Gong, T. Wang, J. He, Chemical Engineering Journal., 2022, 435,134612.
4. J. J. Zhang, F. Tang, K. C. Wan, Y. G. Yang, C. M. Zhang, P. W. Ming, B. Li, J. Mater. Chem. A., 2022,10, 14866-14874.
5. H. Pan, X. L. Wang, F. Y. Li, Q. Xu, J. Mater. Chem. A., 2023, 11, 15006–15013.
6. J. L. Xue, Z. P. Liu, Y. Y. Fan, R. Wang, Y. S. Li, Chemical Engineering Journal., 2023, 476, 146502.

7. X. Zhang, S. Hu, S. Sun, X. Zhang, ChemistrySelect., 2022, 7, e202201503.
8. P. Zhang, Y. Liu, S. Wang, L. Zhou, T. Liu, K. Sun, H. Cao, J. Jiang, X. Wu, B. Li, Small., 2022, 18, 2202725.
9. Sun, Q., Zhu, K., Ji, X.et al. Sci. China Mater., 2022, 65, 1453–1462.
10. A. R. Dong, Y. Lin, Y. Y. Guo, D. D Chen, X. Wang, Y. J. Ge, Q. P. Li, J. J. Qian, Journal of Colloid and Interface Science., 2023, 650, 2056-2064.
11. M. M. Wang, P. Gao, D. Y. Li, X. P. Wu, M. Yang, Z. Q. Li, Y. S. Shen, X. H. Hu, Y. L. Liu, Z. W. Chen, Materials Today Energy., 2022, 28, 101086.
12. M. Gopalakrishnan, M. Etesami, J. Theerthagiri, M. Y. Choi, S. Wannapaiboon, M. T. Nguyen, Y. Yonezawa, So. Kheawhom, Nanoscale., 2022,14, 17908-17920.
13. L.Li, Y. J. Chen, H. R. Xing, et al. Nano Res., 2022, 15, 8056–8064.
14. K. X. Song, Y. Feng, X. Y. Zhou, T. T. Qin, X. Zou, Y. G. Qi, Z. J. Chen, J. C. Rao, Z. Z. Wang, N. L. Yue, X. Ge, W. Zhang, W. T. Zheng, Applied Catalysis B: Environmental., 2022, 316, 121591.
15. J. Ban, X. Wen, H. Xu, Z. Wang, X. Liu, G. Cao, G. Shao, J. Hu, Adv. Funct. Mater., 2021, 31, 2010472.